Laboratory IR spectroscopy of protonated hexa-peri-hexabenzocoronene and dicoronylene

Palotas, J.; Martens, J.; Berden, G.; Oomens, J.

DOI
10.1016/j.jms.2021.111474

Publication date
2021

Document Version
Final published version

Published in
Journal of Molecular Spectroscopy

Journal of Molecular Spectroscopy 378 (2021) 111474

Contents lists available at ScienceDirect

Journal of Molecular Spectroscopy

journal homepage: www.elsevier.com/locate/jms

Laboratory IR spectroscopy of protonated hexa-peri-hexabenzocoronene and dicoronylene

Julianna Palotás [a], Jonathan Martens [a], Giel Berden [a], Jos Oomens [a,b,*]

[a] Radboud University, Institute for Molecules and Materials, FELIX Laboratory, Toernooiveld 7, 6525ED Nijmegen, the Netherlands
[b] van 't Hoff Institute for Molecular Sciences, University of Amsterdam, Science Park 904, 1098XH Amsterdam, the Netherlands

ARTICLE INFO

Article history:
Received 28 January 2021
In revised form 6 April 2021
Accepted 12 April 2021
Available online 26 April 2021

Keywords:
Molecular ions
Vibrational spectroscopy
Interstellar molecules
Polycyclic aromatic hydrocarbon

ABSTRACT

The mid-infrared emission spectra of a large variety of astronomical objects are dominated by the aromatic infrared bands (AIBs), which are now widely accepted to originate from gaseous polycyclic aromatic hydrocarbons (PAHs). It is believed that the astrophysically most relevant molecules are at least 40–50 carbon atoms in size. Still, the large majority of laboratory experiments have been performed on smaller PAHs, mainly for reasons of experimental limitations and availability. Here, we show that combination of atmospheric pressure chemical ionization (APCI) with a direct insertion probe (DIP) inlet gives efficient access to larger, ionic PAHs for action spectroscopy studies. We present the gaseous IR spectra of two astrophysically relevant large PAHs, hexa-peri-hexabenzocoronene ($C_{42}H_{19}^{+}$) and dicoronylene ($C_{48}H_{21}^{+}$) in their protonated form. Compared to their radical cation analogs, the protonated species have a lower dissociation threshold as they can expel a neutral hydrogen radical leaving behind the resonance-stabilized radical cation; provided that the mass spectrometer can resolve precursor and product ions at one amu difference, this generates good quality spectra under multiple-photon dissociation conditions. Quantum-chemical computations at the density functional level are used to support experiments. Despite the apparent similarity of different protonation isomers, their IR spectra are predicted to be remarkably distinct. This facilitates a straightforward identification of the isomers formed experimentally. For both species studied, protonation occurs on the peripheral CH moiety in the 'bay region' of the molecules. We compare the spectra of the protonated species with those of their radical cation analogs reported previously and briefly discuss the astrophysical relevance.

1. Introduction

The aromatic infrared bands (AIBs) dominate the mid-infrared emission spectra of a large variety of astronomical objects [1]. These ubiquitous emission features are detected at main wavelengths of 3.3, 6.2, 7.7, 8.6, 11.2, and 12.7 μm and are believed to be due to infrared radiative cooling of polycyclic aromatic hydrocabons (PAHs) [2,3] and their derivatives [4–6,1] after ultraviolet excitation and fast internal conversion [7]. Although neutral and radical cation PAHs have most often been suggested as candidates for the carriers of the AIBs, alternative ionized PAH molecules have also been suggested as possibly interesting constituents of the interstellar medium (ISM) [8,9,5], some of which have also been characterized in the infrared, see e.g. Refs. [10–15]. In contrast to PAH radical cations, protonated PAHs have a closed-shell electronic structure, making them an interesting alternative form of ionized PAHs [9,5]. Their highly reactive radical cation analogs may react rapidly with H atoms and form the closed-shell configuration [9]. Alternatively, protonation of neutral PAHs is possible as well, due to the sizable proton affinities especially for larger PAH species [16].

To possibly identify the PAH family in the ISM or in circumstellar envelopes, laboratory investigations of the molecules are necessary. Various methods have been employed to obtain gas-phase IR spectra of neutral and ionized PAHs. Schlemmer and Saykally were among the first to record true emission spectra of hot PAHs in the fingerprint IR range [17]. Although emission spectra are most relevant for comparison with interstellar spectra, the experimental methods proved to be technically challenging. Hence, most spectra reported to date for isolated ionized PAHs have employed matrix isolation spectroscopy [18,19,14] or IR multiple-photon dissociation (IRMPD) spectroscopy [20–23].

Although the stable and astrophysically most relevant molecules contain at least 40–50 carbon atoms [7,24], spectroscopic

* Corresponding author at: Radboud University, Institute for Molecules and Materials, FELIX Laboratory, Toernooiveld 7, 6525ED Nijmegen, the Netherlands.
E-mail address: j.oomens@science.ru.nl (J. Oomens).

https://doi.org/10.1016/j.jms.2021.111474
0022-2852/

investigation of molecular ions of that size is challenging. First of all, the availability of high-purity samples is limited and costly. Secondly, vaporizing the molecules for gas-phase experiments or matrix deposition requires increasingly high temperatures as the molecular size grows. Moreover, sample consumption in a Knudsen cell is significant, so that the experimental budget may become a limiting factor. For mass spectrometry based techniques, the mass resolution and/or the solubility when using electrospray ionization may become limiting. Theoretical spectroscopic data are available for larger PAHs [5,25], however a critical evaluation of the calculations is not possible without experimental data.

Gas-phase laboratory experiments on larger PAH radical cations have recently become available [22,23,26], but experimental spectra of gaseous protonated PAHs are only available up to the size of coronene [10,12], with a few larger species being studied in matrices[14]. In the studies by Dopfer and coworkers, protonated PAHs were produced using an electrospray ionization (ESI) source – known for its efficient generation of protonated species – from a solution of the PAH in methanol. The limited solubility of PAHs in typical ESI solvents, such as methanol and water, restricts the extension of these experiments to larger PAHs. Although solubility in organic solvents such as toluene is generally much better, the ESI ionization efficiency and stability from such solutions is very poor.

In recent ion spectroscopy investigations of fullerenes, we have explored the use of an atmospheric pressure chemical ionization (APCI) source, which efficiently produces $C_{60}H^+$ and $C_{70}H^+$ [27,28]. In the APCI source, a solution of the fullerene in an organic solvent is nebulized and ionization is achieved with a corona discharge needle at high voltage, producing both the radical cation as well as the protonated fullerene. Here, we employ a different assembly to the APCI source that does not require solvation of the sample at all and that operates at very low sample consumption rates: the direct insertion probe (DIP) [29]. We use it to record gas-phase IRMPD spectra of two astrophysically relevant large PAHs in their protonated form.

Hexa-peri-hexabenzocoronene (HBC, $C_{42}H_{18}$) has a fully benzenoid structure that gives the molecule high photostability [30,31] and makes it a good candidate to contribute to the AIB bands. Previous studies have explored the properties of neutral HBC [32–34] and its cationic and dicationic forms have been studied in the gas-phase as well[35,36].

The dicoronylene (DC, $C_{48}H_{20}$) cation is, to our knowledge, the largest PAH for which a gas-phase IR spectrum has been recorded to date [22]. It has been studied also in its neutral form [37] and theoretical investigations in cationic, anionic and neutral forms [38,39,37] have also been reported. In addition, photo-ionization and photo-fragmentation – and their branching ratio – at VUV wavelengths was recently investigated [40].

We present in this contribution the vibrational spectra of these species in their protonated form and compare the spectra to those of the corresponding radical cation and neutral species. Protonation breaks the high symmetry of the molecules and its effect on the IR spectra is explored. Also, protonation may occur at different sites in the molecule and we use our spectra to nail down the isomeric form of the protonated species.

2. Methods

2.1. Experimental setup

Gas-phase IR multiple-photon dissociation (IRMPD) spectra are measured in a 3-D quadrupole ion trap mass spectrometer (Bruker Amazon Speed ETD). The mass spectrometer is modified to give optical access to the trapped ion cloud and is connected to the beamline of the Free-Electron Laser for Infrared eXperiments (FELIX). The measurement setup is described in detail elsewhere [41].

An atmospheric pressure chemical ionization ion source (Bruker APCI II) with a direct insertion probe inlet (Bruker DP) [42], shown schematically in Fig. 1, is used to produce the protonated species. The APCI source is particularly suitable for studying apolar substances such as PAHs [43,44] and fullerenes [27]. The DIP assembly [42] replaces the spray nebulizer on the standard Bruker APCI ion source.

The DIP has a high sensitivity that enables the study of very small amounts of material, or samples with a low ionization efficiency [42]. Moreover, it is very useful for samples with low solubility that cannot be introduced into the mass spectrometer with the more traditional spray sources, which is particularly useful for the large PAHs studied here. The extremely low sample consumption rate of the DIP source is especially relevant in the investigation of precious materials; a stable ion signal can be sustained for approximately one hour, using less than 0.1 mg of sample.

The dicoronylene sample was purchased from KENTAX GmbH and the hexa-peri-hexabenzocoronene was synthesized by Hans Sanders at the University of Amsterdam. Minute amounts of the solid sample are placed on the single-use glass tube of the direct insertion probe and then introduced into the APCI source by pushing down the slide. In the corona discharge, both the protonated molecules and radical cations are produced. The yield of ions strongly depends on the setting of the vaporization temperature. The heater is set to 370 °C and the sample vapor is carried along by the N_2 nebulizer gas at 3 bar. The corona current is 4 μA. The offset between the spray shield and capillary cap is set to 500 V

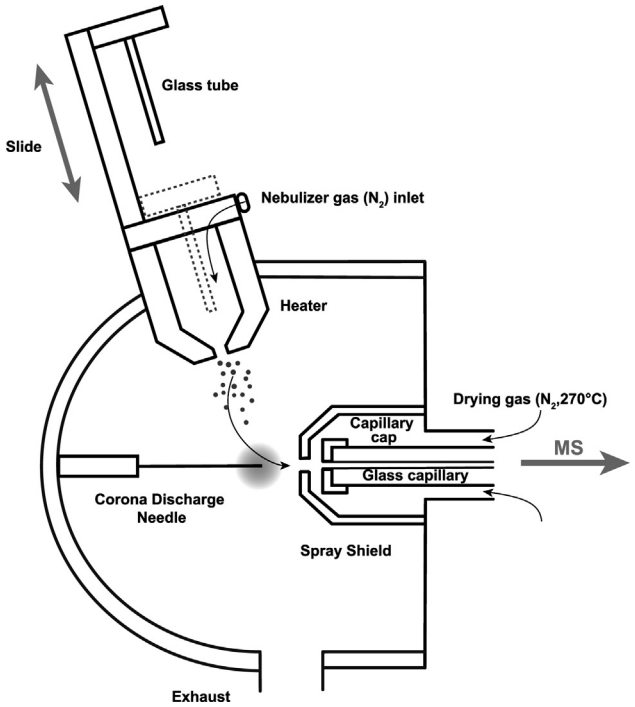

Fig. 1. Sketch of the atmospheric pressure chemical ionization (APCI) source with a direct insertion probe (DIP) inlet. The DIP is mounted on the vaporizer heater. The small amount of solid sample is placed at the end of the glass tube that slides into the heater. In the heater and under the influence of the heated nebulizer gas, the sample sublimates from the surface of the tube. The gas stream reaches the corona discharge where the molecules become ionized at atmospheric pressure, forming both the radical cation as well as protonated species. The ions enter the mass spectrometer through a metal-coated glass capillary covered by the capillary cap.

and the potential of the capillary cap is set to −4500 V, relative to the grounded heater assembly.

For dicoronylene, the protonated and radical cations are present at *m*/z 597 and 596. For hexa-peri-hexabenzocoronene, these peaks appear at *m*/z 523 and 522, as shown in Fig. 2b and e. The *m*/z of the protonated ion of interest is isolated in the trap using the MS/MS features of the mass spectrometer, however, the selected peak is a superposition of the protonated PAH and the ^{13}C-isotopologue of the radical cation. Upon moderately intense IR irradiation, the protonated species undergo dissociation by loss of an H-atom; the radical cations typically require much higher laser powers to dissociate and this does not occur under the experimental conditions set for the protonated species, i.e. typically 5 or 8 dB laser attenuation. Hence, irradiation of the mass-isolated ions with an increasing number of IR pulses leads to a non-zero plateau in the precursor ion depletion curve, see Fig. 2c and f; the remaining ion intensity reveals the percentage of radical cations[45]. For the settings used here, this number is about 15% for dicoronylene and 10% for hexa-peri-hexabenzocoronene.

2.2. IRMPD spectroscopy

IR spectra of the protonated PAHs are obtained by irradiating the trapped and mass-isolated ions (*m*/z 523 for HBC and *m*/z 597 for DC) with the tunable IR light from FELIX. After irradiation, a mass spectrum is recorded, where six mass spectra are averaged at every wavelength. The laser is tuned in steps of 3 cm^{-1}. To generate an IRMPD spectrum, the wavelength-dependent fragmentation yield $Y(\lambda)$ is calculated [46]:

$$Y(\lambda) = \frac{I_{fragment}}{(1-x)\cdot[I_{parent} + I_{fragment}]} \quad (1)$$

where x marks the fraction of radical cations. The fragment fluence ($S(\lambda)$) is then calculated as

$$S(\lambda) = -\ln(1-Y) \quad (2)$$

and corrected linearly for the laser pulse energy and for the irradiation time (i.e. the number of IR pulses). Spectra are then normalized to one.

The vibrational spectra were measured between 6 μm and 14 μm. Laser pulse energies reach up to 120 mJ in this region; at many of the absorption bands in the spectrum, this induces 100% depletion of the protonated PAH population, which would cause saturation in the IRMPD spectrum. Spectral scans were therefore recorded with the laser power attenuated by 5 or 8 dB. The laser produces 7 μs long IR pulses at a 10 Hz repetition rate, which consist of ps micropulses at a 1 GHz repetition rate. The wavelength was calibrated with a grating spectrometer with an accuracy of ±0.01 μm.

2.3. Computational methods

Quantum-chemical calculations were performed using density functional theory (DFT) with the B3LYP/6-311++G(d,p) functional and basis set, which is known to perform reliably in the prediction of IR spectra of large aromatic molecules. In the geometry optimization, no symmetry was imposed to avoid negative frequencies. Point groups referred to in the text correspond to the closest symmetry group of the structures. All computed structures shown correspond to true minima on the potential energy surface.

Vibrational frequencies were computed within the harmonic approximation and scaled by a factor of 0.978. The calculated stick spectra were convoluted using a Gaussian lineshape function with 20 cm^{-1} full width at half maximum (FWHM) to produce computed spectra that can be matched against the experimental ones. In addition, band centers were manually derived from the convoluted spectra as listed in Tables 2 and 3. A listing of the (unscaled) computed frequencies and intensities for each of the isomers of DC + H$^+$ and HBC + H$^+$ is appended in the Supplementary Information.

All energies reported refer to Gibbs free energies. Zero-point energies as well as enthalpies and entropies at 298 K were derived from the unscaled harmonic vibrational frequencies from the B3LYP calculations. At the B3LYP optimized geometry, additional single-point calculations of the electronic energy were performed using Moller–Plesset perturbation theory (MP2) with the 6-311++G(d,p) basis set; Gibbs free energies were then derived using the thermal corrections from the B3LYP calculations. These values were used to further verify the relative energies of the different protonation isomers for each of the two species investigated.

All calculations used the Gaussian16 Rev. A.03 software package installed at the Cartesius supercomputer at SURFsara in Amsterdam.

3. Results and discussion

3.1. Vibrational spectra

Fig. 3 presents the experimental IRMPD spectra of protonated HBC and DC, compared to the IRMPD spectra of their radical cation analogs taken from Refs. [36,22] and to spectra for neutral HBC and DC obtained from the NASA Ames PAH database [47,48]. In general, we observe narrower bands for the protonated systems as com-

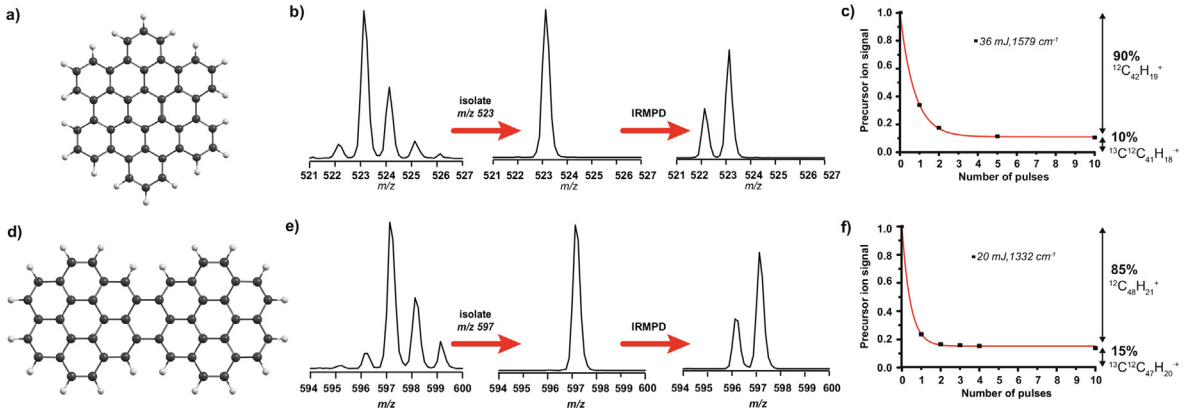

Fig. 2. a) Structure of hexa-peri-hexabenzocoronene (HBC) $C_{42}H_{18}$. **b)** Mass spectrum of HBC as produced in the DIP-APCI source. After isolating the *m*/z 523 peak, loss of an H-atom occurs under resonant irradiation with the IR laser. **c)** Ion depletion curve of HBC + H$^+$. **d)** Structure of dicoronylene (DC), $C_{48}H_{20}$. **e)** Mass spectrum of DC as produced in the DIP-APCI source **f)** Ion depletion curve of DC + H$^+$.

Table 1
Relative Gibbs energies in kJ mol^{-1} of protonated hexa-peri-hexabenzocoronene and dicoronylene, calculated at the B3LYP/6-311++G(d,p) and single-point MP2/6-311++G(d,p)//B3LYP/6-311++G(d,p) levels of theory. The protonation sites labelled by A through E are indicated in Figs. 3 and 4.

	HBC + H^+			DC + H^+	
	B3LYP	MP2@B3LYP		B3LYP	MP2@B3LYP
A	0	0	**A**	37.6	30.0
B	49.4	49.2	**B**	59.8	57.3
			C	59.3	59.2
			D	40.6	32.7
			E	0	0

Table 2
Experimental band positions for protonated hexa-peri-hexabenzocoronene compared with band centers extracted from the convoluted computed spectra of the two protonation isomers. The harmonic frequencies are calculated at the B3LYP/6-311++G(d,p) level and scaled by 0.978. The experimental versus theoretical root mean square deviations (RMSD) are listed on the last row.

	Protonated hexa-peri-hexabenzocoronene			
Exp	**Computed**			
	A	Δ	**B**	Δ
1590	1594.6	4.6	-	-
1575	1579.8	4.8	1578.5	3.5
1529	1541.6	12.6	1526.1	−2.9
1494	1488.6	−5.4	-	-
1459	1465.1	6.1	1450.4	−8.6
1371	1368.0	−3.0	1389.2	18.2
1316	1329.7	13.7	1325.1	9.1
1286	1285.6	−0.4	-	-
1235	1235.6	0.6	1246.4	11.4
1202	1191.4	−10.6	1217.3	15.3
1154	1156.1	2.1	1115.3	−38.7
1068	1082.6	14.6	1022.1	−45.9
1008	1009.0	1.0	990.1	−17.9
960	961.9	1.9	955.1	−4.9
767	770.7	3.7	777.4	10.4
RMSD		7.37		20.27

Table 3
Experimental band positions for protonated dicoronylene compared with band centers extracted from the convoluted computed spectra of the protonation isomers A through E. The harmonic frequencies are calculated at the B3LYP/6-311++G(d,p) level and scaled by 0.978. The experimental versus theoretical root mean square deviations (RMSD) are listed on the last row.

	Protonated dicoronylene									
Exp	**Computed**									
	A	Δ	**B**	Δ	**C**	Δ	**D**	Δ	**E**	Δ
1589	1610.1	21.1	1615.4	26.4	1602.2	13.2	1600.9	11.9	1604.0	15.0
1562	1566.5	4.5	1577.6	15.6	1573.1	11.1	1569	7.0	1566.6	4.6
1522	1523.0	1.0	1531.0	9.0	1547.0	25.0	1528.4	6.4	1526.3	4.3
1480	1485.2	5.2	1499.0	19.0	1494.7	14.7	1484.9	4.9	1483.2	3.2
1447	1438.7	-8.3	-	-	1436.5	-10.5	1458.8	11.8	1457.3	10.3
1404	-	-	1426.2	22.2	-	-	1395.0	−9.0	1408.3	4.3
1380	-	-	1397.1	17.1	1393.0	13	-	-	1382.4	2.4
1332	1348.6	16.6	1341.7	9.7	1366.8	34.8	1342.8	10.8	1345.0	13.0
1296	1302.1	6.1	1295.1	-0.9	1308.7	12.7	1296.4	0.4	1296.1	0.1
1272	-	-	-	-	-	-	-	-	1273	1.0
1202	1238.1	36.1	1228.2	26.2	1230.2	28.2	1235.5	33.5	1209.7	7.7
1166	1217.8	51.8	1184.5	18.5	1183.7	17.7	1209.4	43.4	1178.1	12.1
1145	1171.3	26.3	1146.7	1.7	1148.8	3.8	1177.5	32.5	1149.3	4.3
1133	-	-	1100.1	-32.9	1102.3	-30.7	1154.2	21.2	-	-
1017	994.0	-23.0	989.5	-27.5	994.8	-22.2	994.7	-22.3	1022.6	5.6
880	892.3	12.3	890.5	10.5	904.7	24.7	893.2	13.2	881.6	1.6
848	851.6	3.6	846.8	-1.2	852.4	4.4	855.5	7.5	852.8	4.8
RMSD		21.92		18.69		19.96		19.72		7.32

pared to the radical cations. The signal-to-noise ratio also appears to be better for the spectra of the protonated systems. Furthermore, the spectrum for protonated HBC shows strong peaks between 1400 and 1700 cm^{-1}, which are suppressed and almost absent in the spectrum of the radical cation. In general, the band positions in the radical cation HBC vibrational spectrum appear slightly red shifted as compared with the protonated HBC.

For DC, we observe similar differences between the IRMPD spectra for the protonated and the radical cation species: narrower peaks, better signal-to-noise and more spectral details. A conspic-

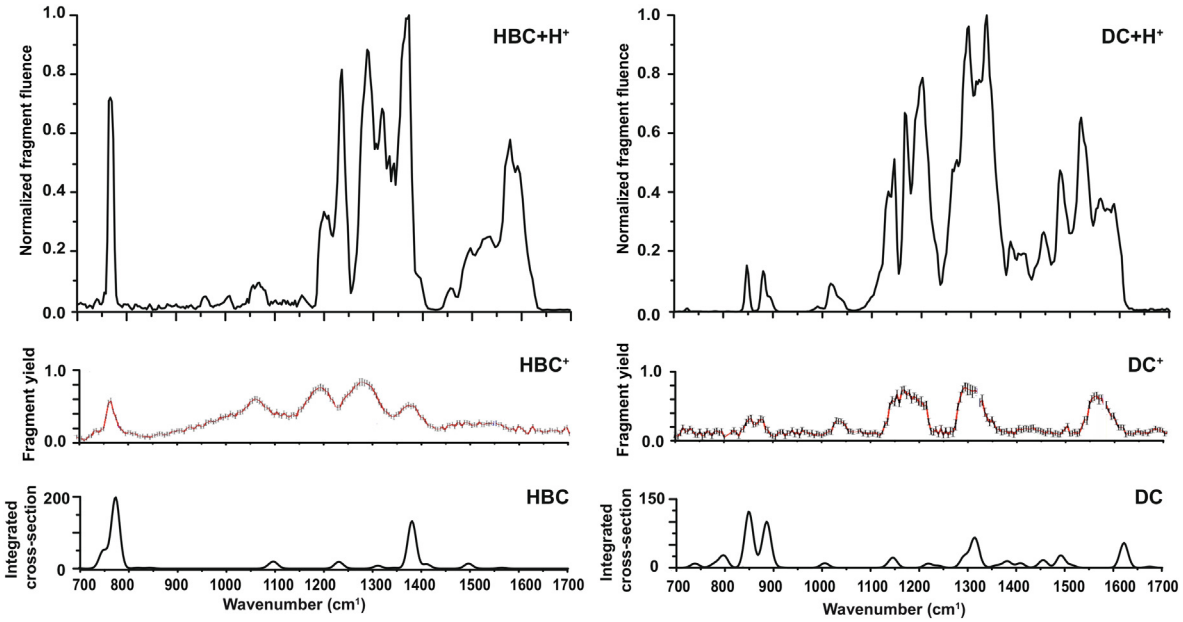

Fig. 3. IRMPD spectra of protonated hexa-peri-hexabenzocoronene (left top) and protonated dicoronylene (right top). The vibrational spectra of the protonated species are compared to the IRMPD spectra of their radical cation counterparts from Refs. [36,22] and to synthetic spectra derived from experimental band positions for the neutral molecules, obtained from the NASA Ames PAH IR Spectroscopic Database (convoluted with 20 cm^{-1} FWHM).

uous difference is the suppressed bands between 1400 and 1500 cm^{-1} in the radical cation spectrum as compared to the significant bands in the protonated system at these wavenumbers.

The vibrational spectra for the neutral species have their strongest bands in the CH out-of-plane bending range. This difference in relative intensities between bands in the long and short wavelength region is a well known characteristic of PAH infrared spectra.[49,18].

The apparent better quality of the IRMPD spectra for the protonated species compared to the radical cations is striking. This may in part be a consequence of the different MS instrumentation used to perform these experiments, but from a methodological viewpoint, we note that the experiments on the protonated species can to some extent be regarded as messenger spectroscopy, where the additional H-atom acts as the messenger tag. The better spectral resolution is attributed to the relatively facile detachment of this tag as a hydrogen radical. Moreover, since this is the only dissociation channel observed under our experimental conditions (Fig. 2e) and and since the mass spectrometer can baseline-resolve a mass difference of one in this mass range, a clean, zero-background IRMPD spectrum is obtained. Although counter to the even-electron rule in mass spectrometry, H-atom detachment is a favorable process with a low dissociation threshold as compared to other dissociation pathways, especially those involving CC bond cleavages, which would reduce the size of the aromatic system. The ionic fragment produced is the radical cation PAH, which is a relatively stable radical due to efficient electron delocalization. Overall, this results in a clean IRMPD spectrum with distinct and fairly well resolved bands, as seen in Fig. 3, which is remarkable given the size of these molecules.

For protonated DC, similar to HBC + H^+, the strongest peaks are present in the shorter wavelength region, where CC stretching with CH bending modes dominate. Weaker bands are visible at 848 and 880 cm^{-1}, corresponding to out-of-plane CH bending modes, and at 1017 cm^{-1}.

3.2. Vibrational spectra and isomer identification

Upon protonation of the two highly symmetric PAH molecules, one or more of several possible isomers may be formed. We assume that protonation occurs through the formation of a CH σ-bond at one of the peripheral CH sites, as was found for smaller protonated PAHs and benzene [50,11,51,12]. Typical barriers for proton migration along the periphery of the PAH molecule have been reported roughly in the range between 50 and 120 kJ mol^{-1} [5,52]. We use quantum-chemical calculations to predict which of the isomers are actually produced in the ion source by matching the IRMPD spectra with computed ones.

The symmetry breaking induced by the added proton gives rise to a very rich vibrational spectrum in case of the large molecules under study. A direct comparison of bands in the observed spectrum with individual computed frequencies is not particularly useful and instead we compare with band centers derived from the convoluted scaled harmonic spectra (see Figs. 4 and 5). Tables 2 and 3 show the band centers in the convoluted computational spectra for each of the protonation isomers of the two molecules, contrasted against the band centers in the experimental IRMPD spectra.

HBC belongs to the D_{6h} point group and upon protonation two isomers are likely to be formed, either having near-C_{2v} (**B**) or near-C_s (**A**) symmetry, as indicated in Fig. 4. The computed vibrational spectra for isomers **A** and **B** are plotted, with the shaded spectrum representing the spectrum convoluted with a 20 cm^{-1} FWHM Gaussian lineshape. By comparing the computed results with the experimental spectrum, it is apparent that the best match is with the lowest-energy configuration, **A**. Although intensities may deviate somewhat between IRMPD and theoretical spectra, the computed band centers reproduce those of the experimental spectrum, which is also clearly confirmed by comparison of the root-mean-square deviation between experimental and theoretical band centers shown in Table 2. The band computed at 1642 cm^{-1}

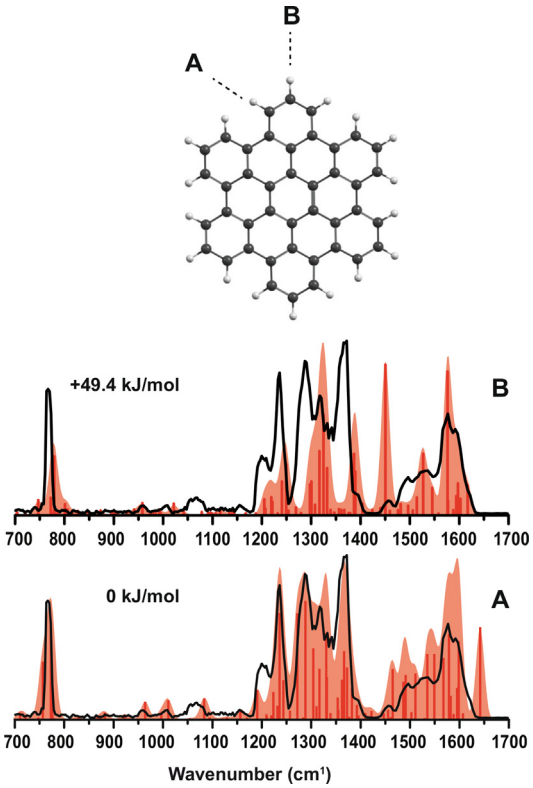

Fig. 4. Experimental spectrum of protonated hexa-peri-hexabenzocoronene (black) compared to computationally predicted spectra for the two isomers obtained by protonation (red), labelled by **A** and **B**. The shaded spectrum represents a 20 cm^{-1} FWHM Gaussian convolution of the stick spectrum. Harmonic frequencies are calculated at the B3LYP/6-311++G(d,p) level and scaled by 0.978. Relative Gibbs energies at the DFT level are shown.

appears absent in the experimental spectrum, although it is a pronounced band in the computed spectrum with an intensity of 120 km/mol (see Supplementary Table 8). The corresponding normal mode is an unusually localized CC-stretch of the peripheral CH–CH bond adjacent to the protonation site. We speculate that the predicted frequency is slightly too high, so that the barely resolved shoulder just above 1600 cm^{-1} in the IRMPD spectrum may correspond to this band. As shown also in Table 1, isomer **B** is computed to be nearly 50 kJ mol^{-1} less stable and would therefore not be expected to be populated at room temperature, in line with our conclusion based on the IR spectrum.

At first glance, the overall IRMPD spectrum of protonated HBC appears fairly typical for (large) cationic PAHs. A strong peak at 767 cm^{-1} is due to the out-of-plane CH vibrations of the trio hydrogen atoms [36] and at shorter wavelengths, roughly 1150 – 1650 cm^{-1}, a series of strong bands is observed, which can be classified as modes with mixed CC stretching and in-plane CH bending character. However, deviations from typical PAH cation spectra are observed upon closer inspection. In the range between 950 and 1100 cm^{-1}, three low-intensity bands are observed, well reproduced by the calculation for isomer **A**. These bands are due to in-plane ring deformation modes with particular contribution from CC stretching of the C–C single bonds to the left and right of the protonated C-atom. Furthermore, a particularly strong band is observed near 1360 cm^{-1}, which according to the calculations is due to a number of unresolved vibrational modes having strong CH_2 scissoring character at the protonation site.

Dicoronylene belongs to the D_{2h} point group and the protonation sites **A** through **E** considered here are shown in Fig. 5. Protonation lowers the symmetry of all isomers to C_s. The computed

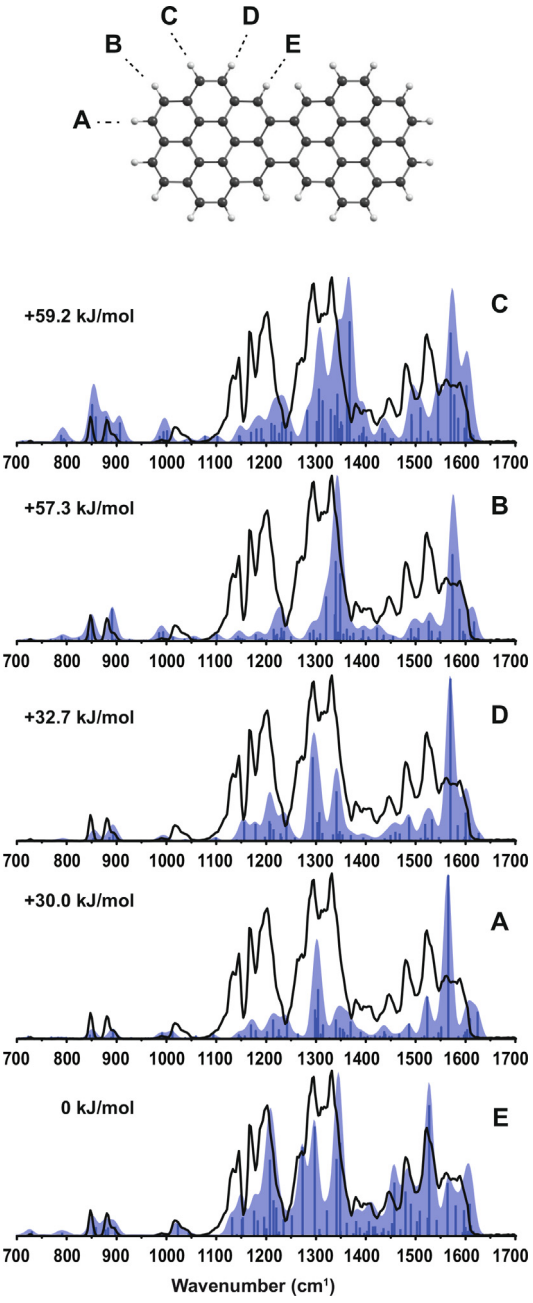

Fig. 5. Experimental spectrum of protonated dicoronylene (black) compared to computationally predicted spectra of its five protonation isomers (blue) labelled **A** through **E**. The shaded spectrum represents a 20 cm^{-1} FWHM Gaussian convolution of the stick spectrum. Harmonic frequencies are calculated at the B3LYP/6-311++G (d,p) level and scaled by 0.978. Relative Gibbs energies at the DFT level are shown for each isomer.

spectra for the five isomers are remarkably distinct and the best spectral match is clearly obtained with the spectrum computed for isomer **E**, as also confirmed by the more detailed comparison in Table 3. This isomer indeed corresponds to the lowest-energy protonated species, with the alternative isomers **A** through **D** lying at least 30 kJ mol^{-1} higher in energy (see Table 1).

Also here, the spectrum appears roughly typical of that of cationic PAHs. In the long wavelength range, two bands are observed which can be attributed to CH out-of-plane modes of the duo-CH moieties (848 cm^{-1}) and the mono-CH moieties (880 cm^{-1}). Some broadening of these bands is due to the slightly different frequencies of these modes on each of the coronene-like subunits of the

molecule, one being perturbed by the protonation and the other not. The band just above 1000 cm^{-1}, due to in-plane CC-stretch and CH-bending, is interesting because it is reproduced correctly only by the calculation for isomer **E**; note a similar band in the spectrum of HBC + H^+. Somewhat in contrast to HBC + H^+, significant bands are observed between 1100 and 1200 cm^{-1}, which have predominantly CH in-plane bending character with varying degrees of CH_2 wagging at the protonation site mixed in. As we move to higher frequencies, we encounter the strongest bands of this system, roughly between 1250 and 1350 cm^{-1}, having mixed CH in-plane bending and CC-stretching character, as is typical for cationic PAH systems. What follows is a series of weaker features, where especially the band at 1380 cm^{-1} has strong CH_2-scissoring character. The absolute computed intensity of these bands is similar to the analog CH_2 scissoring modes in HBC + H^+, although they are much less pronounced in DC + H^+ due to the much higher intensities of the nearby features in DC + H^+. A large number of modes with predominant CC-stretching character is observed between 1400 and 1620 cm^{-1}, whose convoluted contour matches the experimental spectrum fairly closely. Qualitatively, we notice that the normal mode displacements are often larger on the protonated coronene unit and smaller on the unprotonated unit, or vice versa, which may induce significantly larger dipole derivatives and explain the larger band intensities for DC + H^+ as compared to HBC + H^+ (see Supplementary Tables 8–14).

4. Astrophysical considerations and conclusions

The IR spectra presented in this contribution represent, to our knowledge, the first gaseous IR spectra of protonated PAHs significantly larger in size than coronene, approaching the size range relevant in the PAH hypothesis.[1] Therefore, we show in Fig. 6 the two experimental spectra compared with the emission spectrum from the Iris nebula (NGC 7023), which clearly exhibits the typical aromatic emission features.

In line with earlier predictions by Hudgins et al.[5] and with experimental spectra for smaller protonated PAHs recorded in our laboratory[12], we observe that the highest frequency CC-stretching bands are close to the 6.2 μm peak in the interstellar spectrum, indeed closer than what is typically observed in IRMPD spectra for radical cation PAHs. On the other hand, the CC-stretching modes appear to be more dispersed over the 6 to 7 μm range, in contrast to spectra of radical cation PAHs and interstellar emission spectra; compare for instance the spectra of DC^+ and DC + H^+ in Fig. 3. This additional intensity that falls in between the main interstellar bands at 6.2 and 7.6 μm, is also prominently observable in the IRMPD spectra of protonated acenes and coronene[12]. Detailed analyses of astronomical spectra of a variety of objects have revealed many weaker emission features and shoulders in this wavelength range, see *e.g.* Ref. [6].

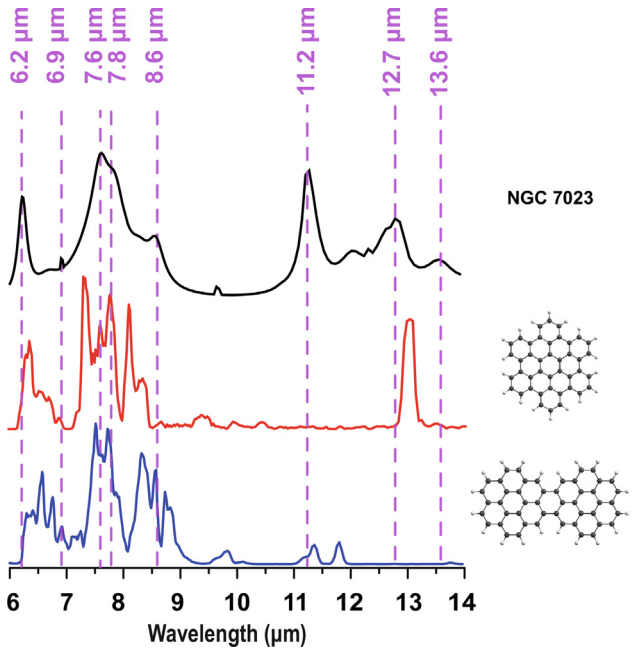

Fig. 6. The vibrational spectra of protonated HBC (red) and DC (blue) compared to the emission spectrum from the Iris nebula (NGC 7023). Dashed lines indicate the aromatic features of the emission spectrum [53].

In the IRMPD spectra, modes with significant CH_2-scissoring character give rise to an observable band near 1380 cm^{-1} that is at best in the wings of the strong 7.6 μm interstellar emission feature. One might have expected that this band would be of relatively low intensity because of the single CH_2 oscillator versus many CH oscillators in large, singly protonated PAHs; this appears to be indeed the case for DC + H^+, but not for HBC + H^+, calling for further studies involving a larger set of systems. The out-of-plane CH-bending modes remain in their typical wavelength ranges of approximately 850–950 cm^{-1} for solo, 800–870 cm^{-1} for duet and 750–810 cm^{-1} for trio moieties[19].

We have presented what we believe are the first gas-phase experimental IR spectra of protonated PAHs in the size range relevant to the PAH hypothesis. The employed action spectroscopy technique involves monitoring the IR-induced dissociation into a single and relatively low-threshold channel (H radical loss), giving remarkably well-resolved vibrational spectra for species of this size.

The added proton has significant influence on the observed spectra, which has been reflected upon in the light of a typical interstellar aromatic emission spectrum. Very interestingly, quantum-chemical computations predict drastically distinct spectra depending on the site of protonation. This allows for an unambiguous assignment of the protonation isomer formed in the experiment, which indeed corresponds to the isomer of lowest energy for both systems investigated. In both cases, protonation occurs on the peripheral CH site in the 'bay region' of the molecules; other protonation isomers are found to be at least 30 kJ mol^{-1} higher in energy.

CRediT authorship contribution statement

Julianna Palotás: Conceptualization, Data curation, Formal analysis, Investigation, Writing - original draft, Writing - review & editing. **Jonathan Martens:** Investigation, Methodology, Writing - review & editing. **Giel Berden:** Investigation, Methodology, Supervision, Writing - review & editing. **Jos Oomens:** Conceptualization, Funding acquisition, Methodology, Supervision, Writing - original draft, Writing - review & editing.

Declaration of Competing Interest

The authors declare that they have no known competing financial interests or personal relationships that could have appeared to influence the work reported in this paper.

Acknowledgements

We sincerely thank Prof. Stephan Schlemmer for his friendship over the past 20 years and the many fruitful collaborations and discussions on laboratory astrochemistry, ion trap mass spectrometry, PAHs and numerous other topics. We gratefully acknowledge the

Nederlandse Organisatie voor Wetenschappelijk Onderzoek (NWO) for the support of the FELIX laboratory. This work is supported by the European MCSA ITN network 'EUROPAH' (Grant No. 722346) and the Dutch Astrochemistry Network (DAN-II, Grant No. 648.000.030) of NWO. For the computational work, we acknowledge support by NWO Exact and Natural Sciences under the 'Rekentijd' program (Grant No. 2019.062) and the SURFsara staff.

Appendix A. Supplementary material

Supplementary data associated with this article can be found, in the online version, at https://doi.org/10.1016/j.jms.2021.111474.

References

[1] A. Tielens, Interstellar polycyclic aromatic hydrocarbon molecules, Annu. Rev. Astron. Astrophys. 46 (2008) 289–337, https://doi.org/10.1146/annurev.astro.46.060407.145211.
[2] W. Schutte, A. Tielens, L. Allamandola, Theoretical modeling of the infrared fluorescence from interstellar polycyclic aromatic hydrocarbons, Astrophys. J. 415 (1993) 397–414, https://doi.org/10.1086/173173.
[3] D. Cook, R. Saykally, Simulated infrared emission spectra of highly excited polyatomic molecules: a detailed model of the PAH-UIR hypothesis, Astrophys. J. 493 (1998) 793–802, https://doi.org/10.1086/305156.
[4] D. Beintema, M. Van den Ancker, F. Molster, L. Waters, A. Tielens, C. Waelkens, T. De Jong, T. de Graauw, K. Justtanont, I. Yamamura, et al., The rich spectrum of circumstellar PAHs, Astron. Astrophys. 315 (1996) L369–L372.
[5] D.M. Hudgins, C.W. Bauschlicher Jr, L.J. Allamandola, Closed-shell polycyclic aromatic hydrocarbon cations: a new category of interstellar polycyclic aromatic hydrocarbons, Spectrochim. Acta A Mol. Biomol. Spectrosc. 57 (2001) 907–930, https://doi.org/10.1016/S1386-1425(00)00453-4.
[6] E. Peeters, S. Hony, C. Van Kerckhoven, A.G.G.M. Tielens, L.J. Allamandola, D.M. Hudgins, C.W. Bauschlicher, The rich 6 to 9 μm spectrum of interstellar PAHs, Astron. Astrophys. 390 (2002) 1089–1113, https://doi.org/10.1051/0004-6361:20020773.
[7] L. Allamandola, A. Tielens, J. Barker, Interstellar polycyclic aromatic hydrocarbons: the infrared emission bands, the excitation/emission mechanism, and the astrophysical implications, Astrophys. J. Suppl. Ser. 71 (1989) 733–775, https://doi.org/10.1086/191396.
[8] V. Le Page, Y. Keheyan, V.M. Bierbaum, T.P. Snow, Chemical constraints on organic cations in the interstellar medium, J. Am. Chem. Soc. 119 (1997) 8373–8374, https://doi.org/10.1021/ja971330v.
[9] T.P. Snow, V. Le Page, Y. Keheyan, V.M. Bierbaum, The interstellar chemistry of PAH cations, Nature 391 (1998) 259–260, https://doi.org/10.1038/34602.
[10] U.J. Lorenz, N. Solcà, J. Lemaire, P. Maitre, O. Dopfer, Infrared spectra of isolated protonated polycyclic aromatic hydrocarbons: Protonated naphthalene, Angew. Chem. Int. Ed. 46 (2007) 6714–6716, https://doi.org/10.1002/anie.200701838.
[11] A. Ricks, G. Douberly, M. Duncan, The infrared spectrum of protonated naphthalene and its relevance for the unidentified infrared bands, Astrophys. J. 702 (2009) 301–306, https://doi.org/10.1088/0004-637X/702/1/301.
[12] H. Knorke, J. Langer, J. Oomens, O. Dopfer, Infrared spectra of isolated protonated polycyclic aromatic hydrocarbon molecules, Astrophys. J. 706 (2009) L66–L70, https://doi.org/10.1088/0004-637X/706/1/L66.
[13] H. Alvaro Galué, J. Oomens, On the electronic structure of isolated monodehydrogenated polyaromatic hydrocarbon ions and their astrophysical relevance, Astrophys. J. 746 (2012) 83, https://doi.org/10.1088/0004-637X/746/1/83.
[14] M. Tsuge, M. Bahou, Y.-J. Wu, L. Allamandola, Y.-P. Lee, The infrared spectrum of protonated ovalene in solid para-hydrogen and its possible contribution to interstellar unidentified infrared emission, Astrophys. J. 825 (2016) 96, https://doi.org/10.3847/0004-637X/825/2/96.
[15] M. Tsuge, C.-Y. Tseng, Y.-P. Lee, Spectroscopy of prospective interstellar ions and radicals isolated in para-hydrogen matrices, Phys. Chem. Chem. Phys. 20 (2018) 5344–5358, https://doi.org/10.1039/c7cp05680j.
[16] D.K. Bohme, PAH and fullerene ions and ion/molecule reactions in interstellar and circumstellar chemistry, Chem. Rev. 92 (1992) 1487–1508.
[17] S. Schlemmer, D. Cook, J. Harrison, B. Wurfel, W. Chapman, R. Saykally, The unidentified interstellar infrared bands: PAHs as carriers?, Science 265 (1994) 1686–1689, https://doi.org/10.1126/science.11539830.
[18] J. Szczepanski, M. Vala, Infrared frequencies and intensities for astrophysically important polycyclic aromatic hydrocarbon cations, Astrophys. J. 414 (1993) 646–655, https://doi.org/10.1086/173110.
[19] D.M. Hudgins, L.J. Allamandola, Interstellar PAH emission in the 11–14 micron region: new insights from laboratory data and a tracer of ionized PAHs, Astrophys. J. 516 (1999) L41–L44, https://doi.org/10.1086/311989.
[20] J. Oomens, A.G.G.M. Tielens, B.G. Sartakov, G. von Helden, G. Meijer, Laboratory infrared spectroscopy of cationic polycyclic aromatic hydrocarbon molecules, Astrophys. J. 591 (2003) 968–985, https://doi.org/10.1086/375515.
[21] J. Oomens, B.G. Sartakov, G. Meijer, G. von Helden, Gas-phase infrared multiple photon dissociation spectroscopy of mass-selected molecular ions, Int. J. Mass Spectrom. 254 (2006) 1–19, https://doi.org/10.1016/j.ijms.2006.05.009.
[22] J. Zhen, A. Candian, P. Castellanos, J. Bouwman, H. Linnartz, A.G.G.M. Tielens, Laboratory gas-phase infrared spectra of two astronomically relevant PAH cations: diindenoperylene, $C_{32}H_{16}^+$ and dicoronylene, $C_{48}H_{20}^+$, Astrophys. J. 854 (2018) 27, https://doi.org/10.3847/1538-4357/aaa7f2.
[23] J. Bouwman, P. Castellanos, M. Bulak, J. Terwisscha van Scheltinga, J. Cami, H. Linnartz, A.G.G.M. Tielens, Effect of molecular structure on the infrared signatures of astronomically relevant PAHs, Astron. Astrophys. 621 (2019) A80, https://doi.org/10.1051/0004-6361/201834130.
[24] J.L. Puget, A. Léger, A new component of the interstellar matter: Small grains and large aromatic molecules, Annu. Rev. Astron. Astrophys. 27 (1989) 161–198, https://doi.org/10.1146/annurev.aa.27.090189.001113.
[25] C.W. Bauschlicher Jr., E. Peeters, L.J. Allamandola, The infrared spectra of very large, compact, highly symmetric, polycyclic aromatic hydrocarbons (PAHs), Astrophys. J. 678 (2008) 316–327, https://doi.org/10.1086/533424.
[26] J. Bouwman, C. Boersma, M. Bulak, J. Kamer, P. Castellanos, A. Tielens, H. Linnartz, Gas-phase infrared spectroscopy of the rubicene cation ($C_{26}H_{14}^+$)-a case study for interstellar pentagons, Astron. Astrophys. 636 (2020) A57, https://doi.org/10.1051/0004-6361/201937013.
[27] J. Palotás, J. Martens, G. Berden, J. Oomens, The infrared spectrum of protonated buckminsterfullerene $C_{60}H^+$, Nat. Astron. 4 (2020) 240–245, https://doi.org/10.1038/s41550-019-0941-6.
[28] J. Palotás, J. Martens, G. Berden, J. Oomens, The infrared spectrum of protonated C_{70}, Astrophys. J. Lett. 909 (2021) L17, https://doi.org/10.3847/2041-8213/abe874.
[29] C. Flego, C. Zannoni, Direct insertion probe- mass spectrometry: A useful tool for characterization of asphaltenes, Energy Fuels 24 (2010) 6041–6053, https://doi.org/10.1021/ef100984y.
[30] J.-I. Aihara, Photochemical stability of polycyclic aromatic hydrocarbons in the interstellar medium, Bull. Chem. Soc. Jpn. 60 (1987) 3143–3147, https://doi.org/10.1246/bcsj.60.3143.
[31] W. Hendel, Z. Khan, W. Schmidt, Hexa-peri-benzocoronene, a candidate for the origin of the diffuse interstellar visible absorption bands?, Tetrahedron 42 (1986) 1127–1134, https://doi.org/10.1016/S0040-4020(01)87517-7.
[32] M. Steglich, C. Jäger, G. Rouillé, F. Huisken, H. Mutschke, T. Henning, Electronic spectroscopy of medium-sized polycyclic aromatic hydrocarbons: implications for the carriers of the 2175 Å UV bump, Astrophys. J. 712 (2010) L16–L20, https://doi.org/10.1088/2041-8205/712/1/l16.
[33] D.L. Kokkin, T.P. Troy, M. Nakajima, K. Nauta, T.D. Varberg, G.F. Metha, N.T. Lucas, T.W. Schmidt, The optical spectrum of a large isolated polycyclic aromatic hydrocarbon: Hexa-peri -hexabenzocoronene, $C_{42}H_{18}$, Astrophys. J. 681 (2008) L49–L51, https://doi.org/10.1086/590207.
[34] G. Rouillé, M. Steglich, F. Huisken, T. Henning, K. Müllen, UV/visible spectroscopy of matrix-isolated hexa-peri-hexabenzocoronene: Interacting electronic states and astrophysical context, J. Chem. Phys. 131 (2009) 204311, https://doi.org/10.1063/1.3266939.
[35] J. Zhen, D. Paardekooper, A. Candian, H. Linnartz, A. Tielens, Quadrupole ion trap/time-of-flight photo-fragmentation spectrometry of the hexa-peri-hexabenzocoronene (HBC) cation, Chem. Phys. Lett. 592 (2014) 211–216, https://doi.org/10.1016/j.cplett.2013.12.005.
[36] J. Zhen, P. Castellanos, J. Bouwman, H. Linnartz, A.G.G.M. Tielens, Infrared spectra of hexa-peri-hexabenzocoronene cations: HBC^+ and HBC^{2+}, Astrophys. J. 836 (2017) 28, https://doi.org/10.3847/1538-4357/836/1/28.
[37] A.L. Mattioda, A. Ricca, J. Tucker, C.W. Bauschlicher, L.J. Allamandola, Far-infrared spectroscopy of neutral coronene, ovalene, and dicoronylene, Astron. J. 137 (2009) 4054–4060, https://doi.org/10.1088/0004-6256/137/4/4054.
[38] G. Malloci, G. Mulas, I. Porceddu, Theoretical spectral properties of PAHs: towards a detailed model of their photophysics in the ISM, J. Phys. Conf. Ser. 6 (2005) 178–184, https://doi.org/10.1088/1742-6596/6/1/020.
[39] G. Malloci, G. Mulas, G. Cappellini, V. Fiorentini, I. Porceddu, Theoretical electron affinities of PAHs and electronic absorption spectra of their mono-anions, Astron. Astrophys. 432 (2005) 585–594, https://doi.org/10.1051/0004-6361:20042246.
[40] G. Wenzel, C. Joblin, A. Giuliani, S. Rodriguez Castillo, G. Mulas, M. Ji, H. Sabbah, S. Quiroga, D. Peña, L. Nahon, Astrochemical relevance of VUV ionization of large PAH cations, Astron. Astrophys. 641 (2020) A98, https://doi.org/10.1051/0004-6361/202038139.
[41] J. Martens, G. Berden, C.R. Gebhardt, J. Oomens, Infrared ion spectroscopy in a modified quadrupole ion trap mass spectrometer at the FELIX free electron laser laboratory, Rev. Sci. Instrum. 87 (2016) 103108, https://doi.org/10.1063/1.4964703.
[42] A. Ballesteros-Gómez, S. Brandsma, J. De Boer, P. Leonards, Direct probe atmospheric pressure photoionization/atmospheric pressure chemical ionization high-resolution mass spectrometry for fast screening of flame retardants and plasticizers in products and waste, Anal. Bioanal. Chem. 406 (2014) 2503–2512, https://doi.org/10.1007/s00216-014-7636-8.
[43] S. Grosse, T. Letzel, Liquid chromatography/atmospheric pressure ionization mass spectrometry with post-column liquid mixing for the efficient determination of partially oxidized polycyclic aromatic hydrocarbons, J. Chromatogr. A 1139 (2007) 75–83, https://doi.org/10.1016/j.chroma.2006.10.086.
[44] L. Guang-Wen, C. Chia-Yang, W. Chang-Fu, Analysis of polycyclic aromatic hydrocarbons by liquid chromatography/tandem mass spectrometry using

atmospheric pressure chemical ionization or electrospray ionization with tropylium post-column derivatization, Rapid Commun. Mass Spectrom. 21 (2007) 3694–3700, https://doi.org/10.1002/rcm.3267.
[45] F.A.M.G. van Geenen, R.F. Kranenburg, A.C. van Asten, J. Martens, J. Oomens, G. Berden, Isomer-specific two-color double-resonance IR^2MS^3 ion spectroscopy using a single laser: Application in the identification of novel psychoactive substances, Anal. Chem. 93 (2021) 2687–2693, https://doi.org/10.1021/acs.analchem.0c05042.
[46] G. Berden, M. Derksen, K.J. Houthuijs, J. Martens, J. Oomens, An automatic variable laser attenuator for IRMPD spectroscopy and analysis of power-dependence in fragmentation spectra, Int. J. Mass Spectrom. 443 (2019) 1–8, https://doi.org/10.1016/j.ijms.2019.05.013.
[47] C. Bauschlicher Jr, C. Boersma, A. Ricca, A. Mattioda, J. Cami, E. Peeters, F.S. De Armas, G.P. Saborido, D. Hudgins, L. Allamandola, The NASA AMES polycyclic aromatic hydrocarbon infrared spectroscopic database: the computed spectra, Astrophys. J. Suppl. Ser. 189 (2010) 341, https://doi.org/10.1088/0067-0049/189/2/341.
[48] C. Boersma, C. Bauschlicher Jr, A. Ricca, A. Mattioda, J. Cami, E. Peeters, F.S. de Armas, G.P. Saborido, D. Hudgins, L. Allamandola, The NASA AMES PAH IR spectroscopic database version 2.00: updated content, web site, and on (off) line tools, Astrophys. J. Suppl. Ser. 211 (2014) 8, https://doi.org/10.1088/0067-0049/211/1/8.
[49] F. Pauzat, D. Talbi, M. Miller, D. DeFrees, Y. Ellinger, Theoretical IR spectra of ionized naphthalene, J. Phys. Chem. 96 (1992) 7882–7886, https://doi.org/10.1021/j100199a011.
[50] G.A. Olah, J.S. Staral, G. Asencio, G. Liang, D.A. Forsyth, G.D. Mateescu, Stable carbocations. 215. ^{13}C nuclear magnetic resonance spectroscopic study of the benzenium, naphthalenium, and anthracenium ions, J. Am. Chem. Soc. 100 (1978) 6299–6308, https://doi.org/10.1021/ja00488a001.
[51] N. Solcà, O. Dopfer, Protonated benzene: IR spectrum and structure of $C_6H_7^+$, Angew. Chem. Int. Ed. 41 (2002) 3628–3631, https://doi.org/10.1002/1521-3773(20021004)41:19<3628::AID-ANIE3628>3.0.CO;2-1.
[52] S. Wiersma, A. Candian, J. Bakker, J. Martens, G. Berden, J. Oomens, W. Buma, A. Petrignani, Photolysis-induced scrambling of PAHs as a mechanism for deuterium storage, Astron. Astrophys. 635 (2020) A9, https://doi.org/10.1051/0004-6361/201936982.
[53] C. Boersma, J.D. Bregman, L.J. Allamandola, Properties of polycyclic aromatic hydrocarbons in the northwest photon dominated region of NGC 7023. I. PAH size, charge, composition, and structure distribution, Astrophys. J. 769 (2013) 117, https://doi.org/10.1088/0004-637x/769/2/117.